Desalination and Water Treatment
www.deswater.com
doi: 10.1080/19443994.2015.1125798

57 (2016) 22081–22098
October

Taylor & Francis
Taylor & Francis Group

Photocatalytic degradation of *p*-nitrotoluene (PNT) using TiO_2-modified silver-exchanged NaY zeolite: kinetic study and identification of mineralization pathway

Praveen K. Surolia[1], Raksh V. Jasra*[2]

Discipline of Inorganic Materials and Catalysis, Central Salt & Marine Chemicals Research Institute, Council of Scientific & Industrial Research (CSIR), G.B. Marg, Bhavnagar 364002, India, email: suroliapv2004@gmail.com (P.K. Surolia), Tel. +91 265 6693935; Fax: +91 265 6693934; email: rvjasra@gmail.com (R.V. Jasra)

Received 12 March 2015; Accepted 19 November 2015

ABSTRACT

Nitroaromatic compounds are suspected hormone disrupter and considered as toxic priority pollutants. In the present study, different amounts of titanium dioxide impregnated zeolite Y (Si/Al ratio 5.5) was modified by silver metal ion exchange and its photocatalytic activity was studied for the mineralization of *p*-nitrotoluene (PNT) in aqueous medium. The synthesized catalysts were characterized by XRD, SEM, inductively coupled plasma, diffuse reflectance spectroscopy, and N_2 adsorption techniques. The analysis of degradation intermediates and mineralization pathways were established using high performance liquid chromatography and mass spectroscopy. The mineralization of PNT into final products: CO_2, H_2O, NO_3^-, and NH_4^+ was assessed by chemical oxygen demand (COD) analysis. Langmuir–Hinshelwood kinetic model was proposed for the degradation and the reaction rate constant values were determined from the experimental data using the model. TiO_2 loading was optimized from the percentage degradation, rate constant, and mineralization values. COD study reveals up to ~60% mineralization in 240 min of irradiation to 75 mg L^{-1} PNT with TiO_2/AgY2 catalyst.

Keywords: Photocatalysis; Mineralization; Degradation; *p*-nitrotoluene; COD; Zeolite

1. Introduction

Aromatic byproducts with low biodegradability released from various chemical industries during their manufacturing processes and their use as chemical intermediates in chemical processes has emerged as major environmental pollutants. Especially nitro and amino groups containing aromatics are toxic in nature [1–3] and inhibit biodegradation of other compounds of waste [4–7]. These pollutants lead to diseases like cyanosis and increased respiratory rate from methamoglobinemia. Regardless of exposure route or

*Corresponding author.

[1]Present address: School of Chemical and Bioprocess Engineering, University College Dublin, Belfield, Dublin 4, Ireland.

[2]Present address: Reliance Technology Group, Reliance Industries Limited, Vadodara Manufacturing Division, Vadodara 391346, India.

length, they affect the blood as the primary target organ and need to be stringently controlled. Complete mineralization of these byproducts is one of the major issues in wastewater pollution. Simplicity and complete mineralization based on the generation of highly reactive hydroxyl radicals [8–10] makes photocatalytic degradation a better alternative to conventional methods for the degradation of organic pollutants in water and air. The photocatalytic decomposition of organic compounds especially from aqueous media has attracted a great deal of attention [7,11–18].

TiO_2 photocatalysis for degradation and mineralization of organic and inorganic pollutants is widely studied [19–23]. The photocatalytic activity of TiO_2 is significantly influenced by its crystallite structure and crystallite size, surface area, porosity, and band gap [24]. The high surface area results in higher catalytic active sites which is vital for efficient adsorption and thus higher photocatalytic activity. This can be achieved by either synthesis of fine TiO_2 particles or dispersion of TiO_2 on a high surface supporting materials, such as zeolite. Furthermore, the intermediates formed during degradation process may be adsorbed and retained for complete mineralization to CO_2 and water. The zeolite framework could also participate actively in electron transfer processes, either as electron acceptor or electron donor for charge separation [25–27].

Adsorption of molecules on porous adsorbents strongly depends on their pore characteristics such as their shape, size, and chemical aspects [28–32]. Zeolites are microporous materials consisting of anionic framework (AlO_2^-) and exchangeable cations with anion–cation pairs from strong electrostatic fields which strongly interact with polar adsorbates [33,34]. These attributes of zeolites make them good adsorbents and supporting materials [35]. Because of the presence of accessible cavities, zeolites can be modified through the incorporation of active species in pores by various techniques such as ion exchange and impregnation [36–39]. Ag^+ ion incorporated and exchanged zeolites have been reported to exhibit higher photocatalytic activity for decomposition, photochemical cleavage of water, photodimerization, photo-oxygen production from water, and photocatalytic degradation of various organic compounds including nitroaromatic compounds and dyes [31,40–56]. The photocatalytic activity of silver-doped titania was found increased significantly for the degradation of oxalic acid, sucrose, methyl orange, and phenol, while the activity was observed mildly enhanced for 4-chlorophenol, 1,4-dicholorobenzene and some dyes [57,58].

In the view of above, we attempt to study the effect of impregnation of titania and silver exchange in zeolite Y for the photocatalytic degradation of *p*-nitrotoluene (PNT). Langmuir–Hinshelwood kinetic model is proposed for the degradation and a possible path for mineralization has been suggested on the basis of identification of a wide range of compounds analyzed by high performance liquid chromatography (HPLC) and ESI–MS [59,60]. Photocatalytic degradation schemes for many aromatic compounds have also been suggested by various studies [48–51,61,62]. Our study is focused on PNT as nitroaromatic compounds are detected as pollutants as a result of their release in industrial effluents [63–66]. The *p*-nitrotoluene (PNT), a common pollutant and a suspected hormone disrupter is formed as an intermediate during the production of trinitrotoluene (TNT). TiO_2 loading was optimized from the percentage degradation, rate constant, and mineralization values.

2. Experimental section

2.1. Chemicals and materials

Titanium(IV) tetraisopropoxide (97%) was procured from Sigma–Aldrich, India. Zeolite NaY with Si/Al ratio 5.5 was procured from United Catalysis India Ltd, India. Silver nitrate, AR grade was procured from Ranbaxy, India and used for the silver ion exchange. Chemical oxygen demand (COD) standard chemical reagents and *p*-nitrotoluene (PNT), AR grade were purchased from E. Merck, India. *p*-aminophenol, *p*-nitrophenol, phenol, and toluene from RANKEM, benzene from Qualigens, India, benzaldehyde, nitrobenzene, benzoic acid, and *p*-toluidine from s. d. fine-chem. Ltd, India, Hydroquinone and benzoquinone from S.D.S. Lab chem. Industry, India were used as standards for HPLC analysis. Deionized distilled water was used for catalyst synthesis as well as for reaction and analysis purposes.

2.2. Synthesis of the catalysts

Synthesis of catalysts was done as described earlier [47]. Prior to the TiO_2 impregnation, zeolite NaY was activated by calcination at 723 K for 4 h under nitrogen flow to remove the water content present in the zeolite cavities. The solutions of calculated amount of titanium tetraisopropoxide for 1, 2, 4, and 10 w/w % TiO_2 in NaY zeolite were prepared in dry ethanol. The solutions were stirred for 30 min followed by the addition of calculated amount of activated zeolite. This slurry was stirred for 2 h and solvent was removed using rotavapour (*Buchi Rotavapour R*-205).

The samples were dried in oven at 393 K for 12 h. The hydrolysis was done by adding water to this sample and dried for a second time in oven at 393 K for 12 h. Thus obtained samples were calcined at 723 K for 11 h. These catalysts were named as TiO_2/NaY1, TiO_2/NaY2, TiO_2/NaY4, and TiO_2/NaY10 for 1, 2, 4, and 10 (w/w %) impregnation of TiO_2 on NaY zeolite, respectively.

TiO_2-impregnated catalysts (2 g) were treated with 5 M silver nitrate solutions at 353 K for 4 h in dark. The residue was filtered and washed with distilled water several times. This cycle was repeated three times. Thus obtained samples were dried at 353 K for 12 h and calcined at 753 K for 6 h. These catalysts were named as TiO_2/AgY1, TiO_2/AgY2, TiO_2/AgY4, and TiO_2/AgY10 for 1, 2, 4, and 10 (w/w %) impregnation of TiO_2, respectively.

2.3. UV irradiation experiments

Photocatalytic degradation of PNT was carried out using two components reactor as reported earlier [7]. First component was inner quartz double wall jacket with inlet and outlet for the water circulation to maintain the temperature of the reaction mixture and second component was outer borosilicate glass container (volume 250 ml after insertion of the inner part). The 125 W mercury vapor lamp (Crompton Greaves Ltd, India) was used as the UV irradiation source. The reaction mixture was continuously stirred by keeping a magnetic stirrer below the reactor and temperature was maintained at 293 K for all the reactions. The photocatalytic activity of the catalysts was evaluated by measuring the decrease in concentration of PNT in the reaction aqueous solution using UV–vis spectroscopy. The calibration curve was plotted for PNT using standard samples of known concentration in distilled water viz. 5, 10, 20, 30, 40, and 50 mg L^{-1}. The absorptions of these samples were measured and the calibration curve was plotted between absorption values with respect to their relevant concentrations. The slope of the curve was calculated and used to determine the PNT concentration using Beer–Lambert's law.

Prior to commencing irradiation, a suspension containing 50 mg of the catalyst and 250 mL of aqueous solution of ca. 30, 50, and 75 mg L^{-1} of PNT was stirred continuously for 30 min in the dark followed by the collection of the 5 mL sample and its analysis to measure the adsorption effect of the catalysts. After the irradiation, 5 ml reaction samples were withdrawn for analysis by a syringe from the irradiated suspension at intervals of 10 min for the first hour and every hour thereafter. The catalysts were separated by centrifugation from the aqueous solution and concentration was determined by UV–vis spectrophotometer (Cary 500, Varian, Palo Alto, CA). The absorbance was measured at λ_{max} 284 nm for PNT. The mineralization of PNT in aqueous solution was confirmed by COD analysis of the samples taken at different reaction time intervals. The detail of COD analysis procedure is described later. Two sets of reactions were performed for each catalyst because of the volume restriction of reaction mixture. First set was for degradation, mineralization, and kinetic study up to 4 h. Second set was to study mineralization pathways up to 24 h (longer time) which was required for complete mineralization and analyze final products.

2.4. Catalyst characterization and analytical methodology

Powder X-ray diffraction patterns were recorded using Cu Kα1 (λ = 0.15405 nm) radiation at 295 K with *Phillips X'pert MPD system*. Diffraction patterns were taken over 2θ range of 5–40° at the scan speed of 0.1°sec^{-1}. The crystallinity of the catalysts was calculated with reference to pure NaY zeolite by taking the average of six major peaks of the catalyst (2θ = 6.28, 15.72, 20.42, 23.70, 27.10, and 31.45).

The Brunauer–Emmett–Teller (BET) surface area, total pore volume of pores (P/P_o = 0.974655453), and adsorption average pore width (4 V/A by BET) of the calcined samples was determined from N_2 adsorption–desorption data measured at 77.4 K using volumetric setup (ASAP 2010, micrometrics, USA).

Diffuse reflectance spectroscopy (DRS) was used to determine the band gap energy as well as the oxidation state of silver in the catalysts. The spectra were taken at room temperature in the range of 225–700 nm by *Shimadzu UV-3101PC* spectrophotometer. The spectrophotometer was equipped with an integrating sphere [67] and $BaSO_4$ was used as a reference.

The morphology of the synthesized catalysts was studied using Scanning Electron Microscopy (Leo Series VP1430) equipped with INCA, Energy Dispersive System (EDX), Oxford instruments. An inductively coupled plasma-optical emission spectrophotometer (Optima 2000 DV, Perkin–Elmer, Eden Prarie, MN) and EDX were used to determine the percentage of Ti and silver metal ion present in the catalyst.

Chemical oxygen demand (COD) was measured using HACH DR 2800 Photometer. The reagents for COD analysis and 3 ml of sample taken at different time were mixed together in glass cells and digested in HACH DRB 200 Thermodigester for two hours at 421 K. After digestion, mixture was cooled down to room temperature and the COD was measured using

the photometer. The COD was measured for both the original PNT solution and the centrifuged reaction samples taken at different time intervals.

The liquid chromatography–mass spectroscopy (LC–MS) experiments were performed on a *Q-Tof micro Y A-260* (Micromass, USA) tandem quadruple–orthogonal Tof instrument, fitted with a lock spray source using Waters Mass Lynx Version 4.0 software.

Samples taken at different times of irradiation were filtered through 0.45 μm filters to remove the catalyst particles before analysis by HPLC-UV at 250 nm. The analysis was carried out using C-18 column 3.5 symmetry (2.1 × 100 mm column). The mobile phase was acetonitrile–water (80:20 v/v) with 1 mL min^{-1} flow rate.

3. Results and discussion

3.1. Structural, textural and electronic properties

Fig. 1(a) shows the X-ray diffraction pattern of TiO_2/NaY and TiO_2/AgY catalysts. The XRD patterns of all TiO_2/AgY and TiO_2/NaY catalysts match with pure NaY zeolite and no extra peak was observed. This indicates that the zeolite framework is unaltered during the TiO_2 impregnation and silver ion-exchange process. However, the crystallinity of the zeolite was found to decrease with increasing amount of impregnated TiO_2 (Table 1). The decrease in crystallinity could be either due to leaching of Al in the zeolite structure [68–70] or due to occupation of cavity pores by TiO_2 particles [71]. The latter seems to be the main reason as leaching of Al from the framework under TiO_2 coating or silver ion-exchange conditions seems unlikely. The diffraction peak due to TiO_2 was not observed in the XRD pattern even at 10% coating, which may be because of high dispersion and low amount of TiO_2 in the zeolite [30].

The BET surface area, total pore volume, and adsorption average pore widthof all catalysts after impregnation of TiO_2 and exchange with Ag^+ ion exchange were observed to decrease as compared to bare NaY zeolite sample (Table 1). This suggests the occupation of zeolite pores by TiO_2 particles. The decrease in the surface area was very high after the Ag^+ ion exchange (Table 1). This decrease may be due to the development of Ag_n^0 and Ag_m^{n+} (size of Ag^+ ion is 1.29 Å as compared to 0.89 Å of Na^+.) species as confirmed by DRS analysis.

The DRS spectra of TiO_2/NaY, TiO_2/AgY, and bare NaY are shown in Fig. 1(b) and (c). All TiO_2/AgY catalysts show a band in wavelength regions larger than 250 nm that is at around 288 and 322 nm. No peak was observed below 250 nm. This shows that

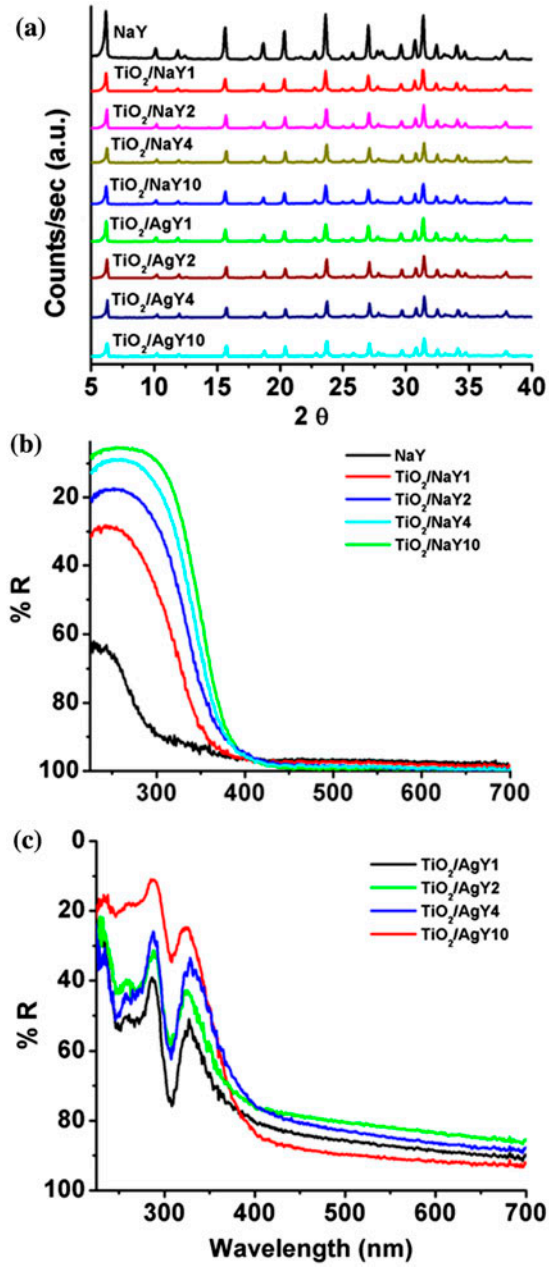

Fig. 1. XRD patters of all synthesized catalysts (a), diffuse reflectance spectra of TiO_2/NaY (b), and TiO_2/AgY zeolite catalysts (c).

silver is present in the form of Ag_n^0 and Ag_m^{n+} clusters and not present as isolated Ag^+ ion. This indicates that the reduction and aggregation of Ag^+ ions have occurred in the zeolite cavities [41,72,73]. This reduction is due to autoreduction process in which O_2 from zeolite framework is released. The reports explained that oxide ions of the zeolite framework could have been oxidized to O_2, and that Ag^+ ions could have

Table 1
Crystallinity, surface area, total pore volume, and adsorption average pore width

Catalyst	Crystallinity (%)	Surface area ($m^2\ g^{-1}$)	Total pore volume ($cm^3\ g^{-1}$)	Adsorption average pore width (Å)
NaY	100	737	0.401135	22.9385
TiO_2/NaY1	99	688	0.383876	22.1734
TiO_2/NaY2	98	682	0.376465	21.3772
TiO_2/NaY4	90	676	0.365324	21.7783
TiO_2/NaY10	87	639	0.327924	20.7576
TiO_2/AgY1	99	506	0.270343	21.8499
TiO_2/AgY2	89	505	0.254417	20.2694
TiO_2/AgY4	80	502	0.251209	19.8327
TiO_2/AgY10	74	494	0.223434	17.6543

been correspondingly reduced [26,74]. However, the absence of band at 410 nm confirms the lack of aggregation of the metallic silver particles up to several nanometer or larger size [41,75–77]. Due to the small amount of TiO_2 in all catalysts, the band edge position and band-gap energies could not be determined from the DRS spectra after taking the differential.

The morphology of synthesized catalysts is shown in Fig. 2. The SEM images confirm that the morphology of the synthesized catalysts was not changed after the silver exchange and particles were hexagonal in shape.

The inductively coupled plasma (ICP) and EDX analysis (Table 2) were used to confirm the percentage loading of Ti and the percentage of Ag^+ ion exchange.

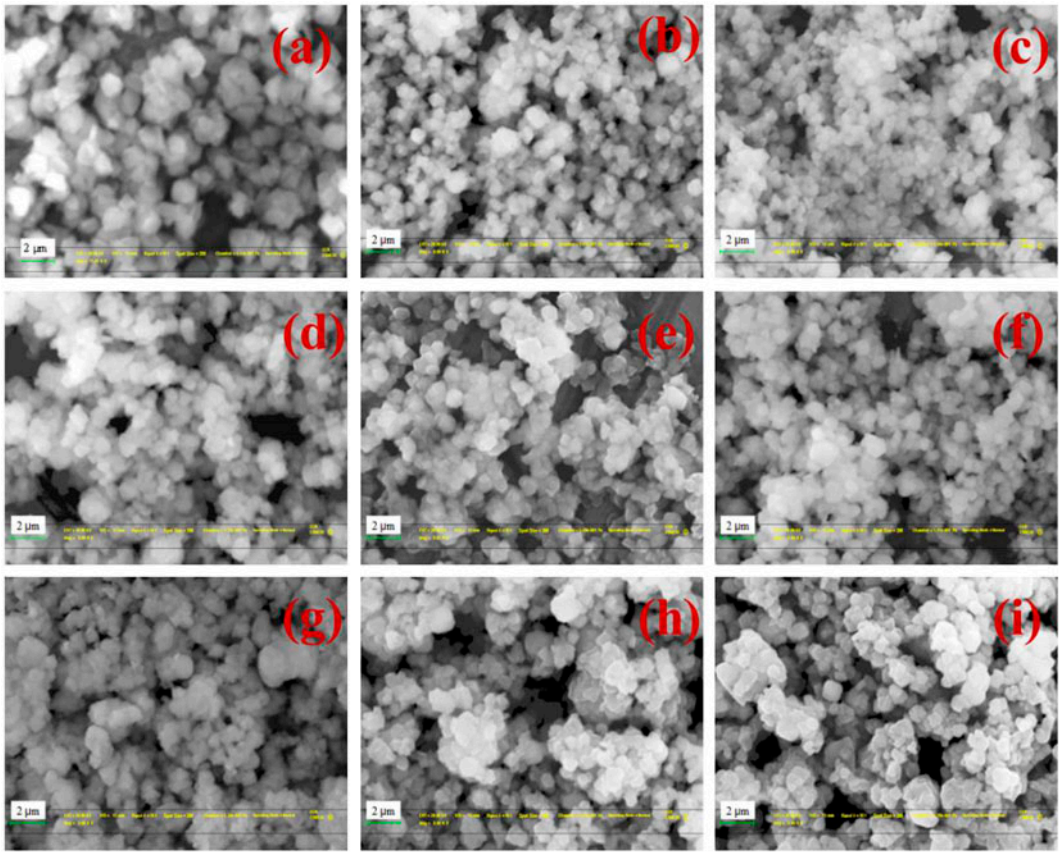

Fig. 2. SEM images of synthesized catalysts: (a) Bare NaY, (b) TiO_2/NaY1, (c) TiO_2/NaY2, (d) TiO_2/NaY4, (e) TiO_2/NaY10, (f) TiO_2/AgY1, (g) TiO_2/AgY2, (h) TiO_2/AgY4, and (i) TiO_2/AgY10.

Table 2
Elemental analysis results by EDX and ICP

Catalysts	Percentage of element (weight %)										
	Na		Ag		Si		Al		Ti		O
	EDX	ICP	EDX	ICP	EDX	ICP	EDX	ICP	EDX	ICP	EDX
NaY	6.23	6.29	–	–	32.48	33.15	5.87	5.90	–	–	52.56
TiO_2/NaY1	6.17	6.25	–	–	28.96	29.13	5.25	5.31	0.62	0.98	53.65
TiO_2/NaY2	6.34	6.35	–	–	28.18	28.68	5.15	5.23	1.28	1.92	55.23
TiO_2/NaY4	6.39	6.22	–	–	27.42	27.89	5.18	5.11	2.89	4.11	56.08
TiO_2/NaY10	6.25	6.12	–	–	26.67	27.24	4.74	4.80	6.08	6.98	56.25
TiO_2/AgY1	5.02	5.16	1.12	1.08	29.44	28.94	5.37	5.31	0.56	0.96	54.74
TiO_2/AgY2	4.94	5.23	1.10	1.05	28.74	28.56	5.22	5.17	1.25	1.86	55.06
TiO_2/AgY4	5.13	5.15	1.15	1.13	28.68	29.25	5.14	5.34	2.83	3.95	56.54
TiO_2/AgY10	5.20	5.20	1.06	1.00	26.06	28.96	4.70	5.18	5.84	6.21	57.14

The loading amount of metal depends upon the porosity of support. Thus the actual amounts of Ti content measured by EDX and ICP analysis are mentioned in Table 2. The results confirm silver ions exchange in zeolite. The Si:Al ratio also found constant with increase in Ti content and silver exchange in zeolite material.

3.2. Photocatalytic activity

The mechanism of the photocatalytic oxidation can be described with consecutive steps initiating with illumination with UV light at the active catalyst surface > TiO_2, generating charge carriers.

$$> TiO_2 \xrightarrow{h\nu} h^+_{VB} + e^-_{CB} \quad (1)$$

$$h^+_{VB} + e^-_{CB} \rightarrow \text{heat} \quad (2)$$

$$> TiO_2 - OH^- (\text{or} > TiO_2\text{–}H_2O) + h^+_{VB} \leftrightarrow > TiO_2\text{–}{}^{\cdot}OH (\text{or} > TiO_2\text{–}{}^{\cdot}OH + H^+) \quad (3)$$

$$> TiO_2 + PNT \leftrightarrow > TiO_2\text{–}PNT \quad (4)$$

$$> TiO_2 + I \leftrightarrow > TiO_2\text{–}I \quad (5)$$

$$> TiO_2 + {}^{\cdot}OH \leftrightarrow > TiO_2\text{–}{}^{\cdot}OH \quad (6)$$

$$> TiO_2\text{–}PNT + h^+_{VB} \rightarrow > TiO_2\text{–}PNT^{\cdot+} \rightarrow \text{Mineralized species} \quad (7)$$

$$> TiO_2\text{–}I + h^+_{VB} \rightarrow > TiO_2\text{–}I^{\cdot+} \rightarrow \text{Mineralized species} \quad (8)$$

$$> TiO_2\text{–}PNT + > TiO_2\text{–}{}^{\cdot}OH \rightarrow > TiO_2 + > TiO_2\text{–}PNT^{\cdot+} + OH^- \rightarrow \text{Mineralized species} \quad (9)$$

$$> TiO_2\text{–}I + > TiO_2\text{–}{}^{\cdot}OH \rightarrow > TiO_2 + > TiO_2\text{–}I^{\cdot+} + OH^- \rightarrow \text{Mineralized species} \quad (10)$$

$$> TiO_2\text{–}PNT + {}^{\cdot}OH \rightarrow > TiO_2\text{–}PNT^{\cdot+} + OH^- \rightarrow \text{Mineralized species} \quad (11)$$

$$> TiO_2\text{–}I + {}^{\cdot}OH \rightarrow > TiO_2\text{–}I^{\cdot+} + OH^- \rightarrow \text{Mineralized species} \quad (12)$$

The generated e^-/h^+ pair can undergo charge transfer to the adsorbate on photocatalyst surface or recombine to each other leading low quantum yield of photocatalytic reaction (step 2). The photocatalyst TiO_2 exist in hydroxylated form in aqueous suspension with coverage of 5–15 OH nm^{-2} [78]. The generated hole can react with these surface hydroxyl group or water to produce strong oxidizing agents hydroxyl radicals (step 3). However, initially the original compounds ("PNT") and later intermediate species ("I") also compete with ·OH radical and can be adsorb on photocatalyst surface (step 4–6) where they can capture the generated hole (step 7–8) as the competition with the step (3). The ·OH radical can attack on adsorbed organic species at catalyst surface which either may be PNT or intermediate. This attacking ·OH radical may be free or adsorbed on catalyst surface (steps 9–12). The kinetics of the organic compound degradation can be determined by the applying elementary stoichiometric balance and steady state approximation on the

Table 3
Kinetic fit results (r_0, k and K) of the experimental data to the Langmuir–Hinshelwood model

Catalyst	Initial rate of reaction ($r_0 \times 10^6$ mol L^{-1} min^{-1})			Reaction rate constant ($k \times 10^6$) (mol L^{-1} min^{-1})	Adsorption constant ($K \times 10^{-3}$) (L mol^{-1})
	2.2×10^{-4} (30 mg L^{-1})	3.7×10^{-4} (50 mg L^{-1})	5.5×10^{-4} (75 mg L^{-1})		
Blank	1.93	2.60	2.87	–	–
NaY	2.06	3.13	3.40	6.08	2.56
TiO_2/NaY1	2.93	3.80	5.23	9.55	1.97
TiO_2/NaY2	3.57	5.00	5.70	9.98	2.56
TiO_2/NaY4	3.32	4.90	5.30	9.86	2.36
TiO_2/NaY10	3.10	4.30	5.10	9.17	2.33
TiO_2/AgY1	4.00	5.87	6.00	10.25	3.00
TiO_2/AgY2	4.53	6.00	6.80	10.48	3.49
TiO_2/AgY4	3.80	5.67	5.80	10.30	2.74
TiO_2/AgY10	3.37	4.93	5.30	9.57	2.53

intermediates and radicals formed during the process. The rate expression obtained by these processes is as expressed in Eq. (A14) as given in Appendix A and The L–H parameters can be evaluated by simplify and linearizing this equation as Eq. (A17). From the equation, we can find the values of reaction kinetic constant "k" and adsorption constant "K". The intercept determines the reaction kinetic constant "k" that varies with the rate of degradation and the value of adsorption constant "K" can be obtained by the slope of the curve. The higher value of k implies the higher rate of degradation.

The photocatalytic activities of the synthesized catalyst were monitored at pH value (5.96–6.00) without addition of any acid or alkali, at catalyst dose of 200 mg L^{-1} and 293 K temperature, while initial concentration of PNT was varied as 30 (2.2×10^{-4} M), 50 (3.7×10^{-4} M) and 75 mg L^{-1} (5.5×10^{-4} M). The values of reaction kinetic constants, adsorption constants and initial rates are listed in Table 3. The initial rates of degradation were determined from the initial slope of the concentration profile.

When the blank study i.e. direct photolysis reaction was carried out (without catalyst), the concentration of PNT was found reduced with low extent and less percentage degradation value (Fig. 3(a)). From the data in Table 3, it is clear that initial rate and final degradation was highest for the reaction using TiO_2/AgY2 catalyst. The percentage degradation was observed 92, 84, and 74% with 30, 50, and 75 mg L^{-1} initial concentration of PNT, respectively, using TiO_2/AgY2 catalyst. These values were highest among all other values observed using other catalysts and the blank study (Fig. 4).

The decrease in the concentrations due to adsorption is reported in Table 4. These values suggested that the adsorption was highest with bare zeolite because of its higher surface area. As the surface area decreases in TiO_2 coated and silver-incorporated catalysts, the adsorption values also decrease compared to bare zeolite. Moreover, the extent of percentage concentration decrease due to adsorption was lowered with the increase in initial concentration of PNT and observed least decrease with 75 mg L^{-1}. Earlier study demonstrates that the activity of the TiO_2 impregnated zeolite is higher than that of synthesized TiO_2 photocatalyst [30]. This is due to the higher surface area and fine dispersion of TiO_2 in cavities of the zeolite which are mainly the responsible factors for the facilitation of higher photocatalytic activity. Fine dispersion on the zeolite surface results in higher photocatalytic active sites on the zeolite surface. Above-mentioned factors of the supported titania results into enhanced concentration of substrate molecules near TiO_2 particles which increases the rate of photocatalysis as compared to the bare TiO_2 catalyst. The reaction sample was analyzed by ICP analysis after the reaction. The absence of exchanged silver and impregnated Ti metal in the reaction sample confirms the lack of leaching of these metals during the reaction.

3.2.1. Effect of substrate concentration

The influence of initial concentration of substrate on degradation and mineralization kinetics of PNT was studied using three different initial concentration, viz., 30, 50, and 75 mg L^{-1} (Table 3). It is clear from the data that as the initial concentration increases, the rate of disappearance of PNT also increases but the final percentage degradation after 4 h decreases as shown in Fig. 4. In all the cases, catalyst TiO_2/AgY2

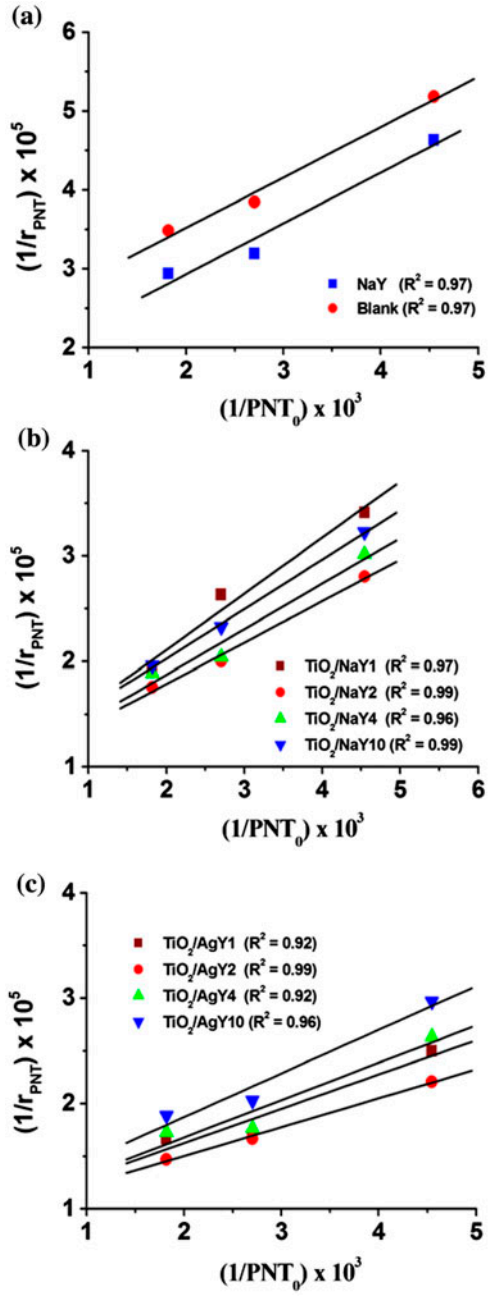

Fig. 3. The Langmuir–Hinshelwood (L–H) plot of the reactions with (a) blank i.e. photolysis and NaY (b) TiO_2/NaY1 to TiO_2/NaY10 and (c) TiO_2/AgY1 to TiO_2/AgY10 catalysts.

exhibited highest photocatalytic activity. Similar results were observed in mineralization processes (Table 5). At higher initial concentration of PNT, all catalytic sites of the semiconductor catalyst surface are occupied by the reactant molecules and the substrate may come to a saturation adsorption. When the

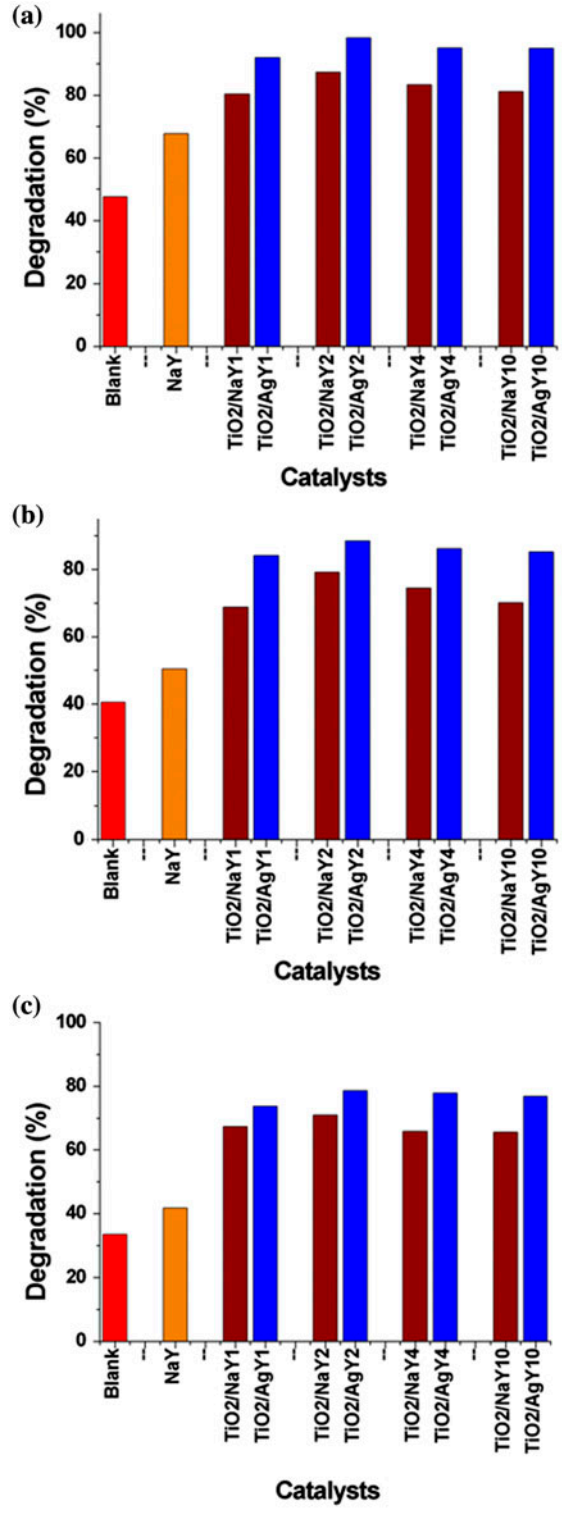

Fig. 4. Percentage degradation of the PNT (a) 30 mg L^{-1}, (b) 50 mg L^{-1}, and (c) 75 mg L^{-1} concentration in the presence of different synthesized catalysts after 4 h reaction.

Table 4
Adsorption properties of the catalysts

Catalyst	Decrease in concentration with adsorption (%) Initial concentration		
	30 (mg L^{-1})	50 (mg L^{-1})	75 (mg L^{-1})
NaY	27	14	10
TiO_2/NaY1	25	12	09
TiO_2/NaY2	24	12	09
TiO_2/NaY4	22	11	09
TiO_2/NaY10	21	11	08
TiO_2/AgY1	16	11	09
TiO_2/AgY2	15	10	08
TiO_2/AgY4	13	10	08
TiO_2/AgY10	12	09	07

substrate concentration was lower than the saturation adsorption concentration, the reaction rate would increase with increasing concentration, and it would decrease after the substrate was higher than the saturation adsorption concentration. Further increase in initial concentration does not affect the actual catalyst surface concentration. Therefore, this dwindle the catalyst surface to reactant ration and may result in the decrease of observed final degradation at higher initial concentration.

Another factor which governs the degradation is generation and migration of the photogenerated e^-/h^+ pair, and reaction between these photogenerated h^+ (·OH radical) and organic substrate molecules. These both processes occur in series and each step may become the rate-determining step for overall process. At low concentration the later process dominants, resulting high degradation values while at high concentration, the former process dominants, and resulting low degradation values. The high concentration reduces the diffusion rate of intermediates from the catalyst surface as well as the transfer rate of the substrate towards catalyst which is another reason for the decrease in the final degradation values.

3.2.2. Effect of TiO_2 concentration

The removal efficiency of PNT was observed to decrease with increased TiO_2 concentration. After certain concentration level, the TiO_2 particles block the pores of zeolite material which results in decrease in adsorption capacity of the catalyst towards organic substrate molecules. This could make the decomposition less effective. According to the principle of the photocatalytic reaction, the main step in process occur on the surface of solid semiconductor photocatalyst, so the adsorption of organic compounds on the catalyst surface certainly affects the reaction and usually high adsorption capacity favors the reaction.

3.2.3. Effect and role of silver

Ag particle in contact with TiO_2 surface can act as e^-/h^+ separation center as the Fermi level of TiO_2 is higher than that of silver metal [79,80]. This makes it feasible to thermodynamically transfer an e^- from conduction band to metallic silver particles, enhancing the e^-/h^+ separation and the subsequent transfer of the trapped e^- to the adsorbed O_2 acting as e^- acceptor [81]. Higher Fermi level of TiO_2 than that of Ag metal results in the formation of Schottky barrier at metal–semiconductor contact region, which improves the stability of charge separation and thus enhance the photocatalytic activity of TiO_2 [57]. There are different oxidizing entities responsible for breaking the bonds of the organic species. These entities may either be hydroxyl radicals [82,83] or valence band holes [84]. The reactor configuration and experimental conditions could play a role in controlling the performance of Ag/TiO_2 [57,85–87]. The different research groups have been reported varied range of sliver loading for the improvement of efficiency [57,87,88]. It was also observed that as Ag loading increases, the photocatalytic efficiency did not improve proportionally. This was due to reduction in the TiO_2 surface active sites available for redox reaction which leads to a decrease in the concentration of photogenerated charge carrier and photocatalytic activity of photocatalyst. This inadvertently reduces the rate of mineralization [89,90]. In this work, we observed all Ag-exchanged catalysts better performed comparative to their respective unexchanged catalysts (Tables 3 and 5). This confirms Ag particles are helping in charge separation and thus photocatalytic activity of catalysts.

3.2.4. Role of zeolite framework

The zeolite with higher surface area increases the adsorption of the substrate and hence increases its efficiency towards degradation by taking h^+. Electron-rich zeolite surface function as h^+ scavenger to stop the e^-/h^+ recombination. This increases the electron donor capacity of TiO_2 site for reduction of adsorbed species [12]. Upon irradiation of TiO_2 on zeolite by UV light, the conduction band electron generated can react with adsorbed PNT from TiO_2 site before charge recombination. The oxygen tetrahedron in zeolite framework has in its center either an atom of silicon, SiO_4^{4-} or aluminum AlO_4^{5-}. Since the charge on the aluminum oxygen tetrahedron is five minus while that on the

Table 5
COD of reaction mixture with respect to irradiation time using different catalysts

Initial concentration	Catalysts	COD (mg L^{-1}) Irradiation time (min)					
		0	30	60	120	180	240
30 mg/L	Blank	69	66	65	60	56	50
	NaY	69	63	61	55	52	45
	TiO_2/NaY1	69	50	47	45	38	33
	TiO_2/NaY2	69	47	44	42	34	28
	TiO_2/NaY4	69	48	46	44	36	31
	TiO_2/NaY10	69	49	48	45	39	36
	TiO_2/AgY1	69	44	42	41	31	26
	TiO_2/AgY2	69	43	40	39	24	23
	TiO_2/AgY4	69	38	37	35	34	29
	TiO_2/AgY10	69	55	48	46	41	40
50 mg/L	Blank	100	96	92	88	82	74
	NaY	100	90	85	78	74	71
	TiO_2/NaY1	100	85	81	76	69	65
	TiO_2/NaY2	100	81	76	70	64	61
	TiO_2/NaY4	100	82	77	73	68	64
	TiO_2/NaY10	100	84	78	74	69	66
	TiO_2/AgY1	100	78	70	69	66	58
	TiO_2/AgY2	100	62	61	57	56	55
	TiO_2/AgY4	100	62	61	60	59	58
	TiO_2/AgY10	100	65	64	61	58	57
75 mg/L	Blank	145	140	132	124	119	115
	Na	145	137	126	118	110	103
	TiO_2/NaY1	145	95	88	81	77	74
	TiO_2/NaY2	145	80	74	72	69	65
	TiO_2/NaY4	145	90	83	79	76	74
	TiO_2/NaY10	145	93	86	79	74	68
	TiO_2/AgY1	145	83	75	73	72	70
	TiO_2/AgY2	145	70	68	64	60	57
	TiO_2/AgY4	145	78	77	74	73	72
	TiO_2/AgY10	145	101	99	93	89	88

silicon tetrahedron is four minus, this excess negative charge on the aluminum tetrahedra is responsible for the electron rich property of the zeolite surface.

3.3. Mineralization

The mineralization during the photocatalytic process of PNT was confirmed by COD value determination (Table 5). The decrease in COD values was found minimum when blank experiment was run, and observed highest when TiO_2/AgY2 was used as a catalyst. The decrease in COD values with the blank study were 28, 26 and 21% while using TiO_2/AgY2 catalyst the observed decrease in the COD values were 67, 45, and 60% with 30, 50, and 75 mg L^{-1} PNT, respectively. The presence of silver ion in zeolite framework was found to increase the mineralization capacity. In all the cases, COD values could not reach to zero in 4 h irradiation. These COD data as well as UV–vis spectra data confirm that an optimum amount of TiO_2 on zeolite material is required for higher photocatalytic activity. However, COD decrease was lower than degradation values observed from UV data. It confirms that some intermediate organic and nitro-i ntermediates are still present in reaction samples.

3.4. Tentative mechanism

The mass spectra were performed for the samples taken at different time intervals of the reactions. Reaction of a suspension containing 50 mg of the TiO_2/AgY2 catalyst and 250 mL of aqueous solution

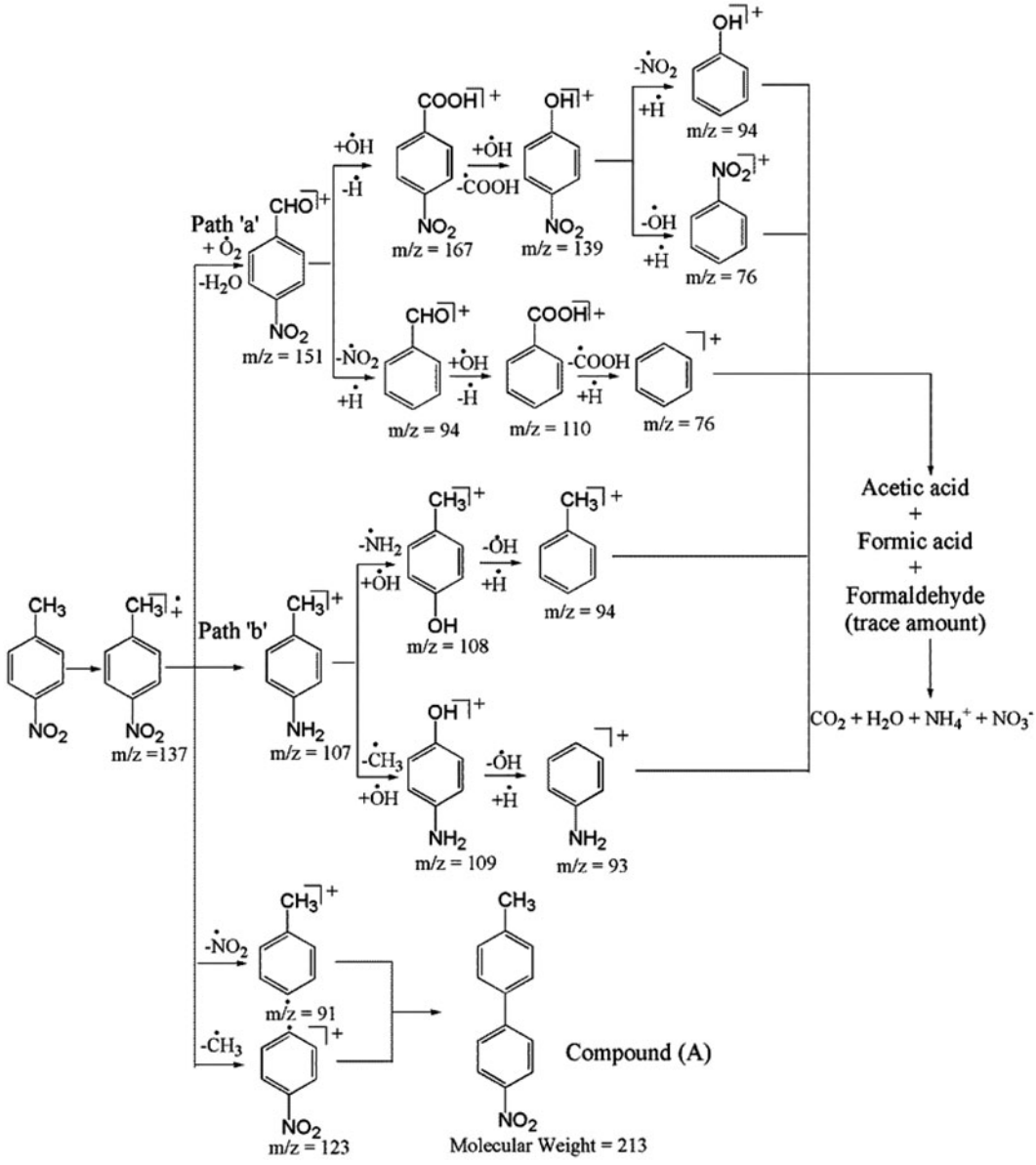

Fig. 5. Proposed fragmentation pattern of *p*-nitrotoluene.

of ca. About 50 mg L^{-1} of PNT was used for this purpose. The m/z values present in these mass spectra are used to propose the major intermediates while the HPLC analysis was used to confirm the major intermediates along with the mass spectra analysis. The different m/z values in the mass spectrum either may be due to the fragmentation of molecular ion peak in the ionization process or the intermediate present in the sample formed during the mineralization process of PNT. This may also be the resultant of both phenomena, however, these are considered to propose a mechanism assuming the intermediates of these m/z values are formed during the mineralization in some or more quantity. Few of these proposed intermediates are confirmed by HPLC using their standard sample solutions.

The HPLC analysis was carried out to confirm the intermediates suggested in the proposed fragmentation pathway. The compounds were confirmed on the basis of their retention time in the HPLC analysis. The suggested intermediates which were defined are nitrobenzene, 4-aminophenol, benzoic acid, benzaldehyde, 4-aminotoluene, toluene, benzoquienone, and hydroquinone. However, all the compounds could not be confirmed as their standards were not available. The HPLC analysis revealed that, after few minutes

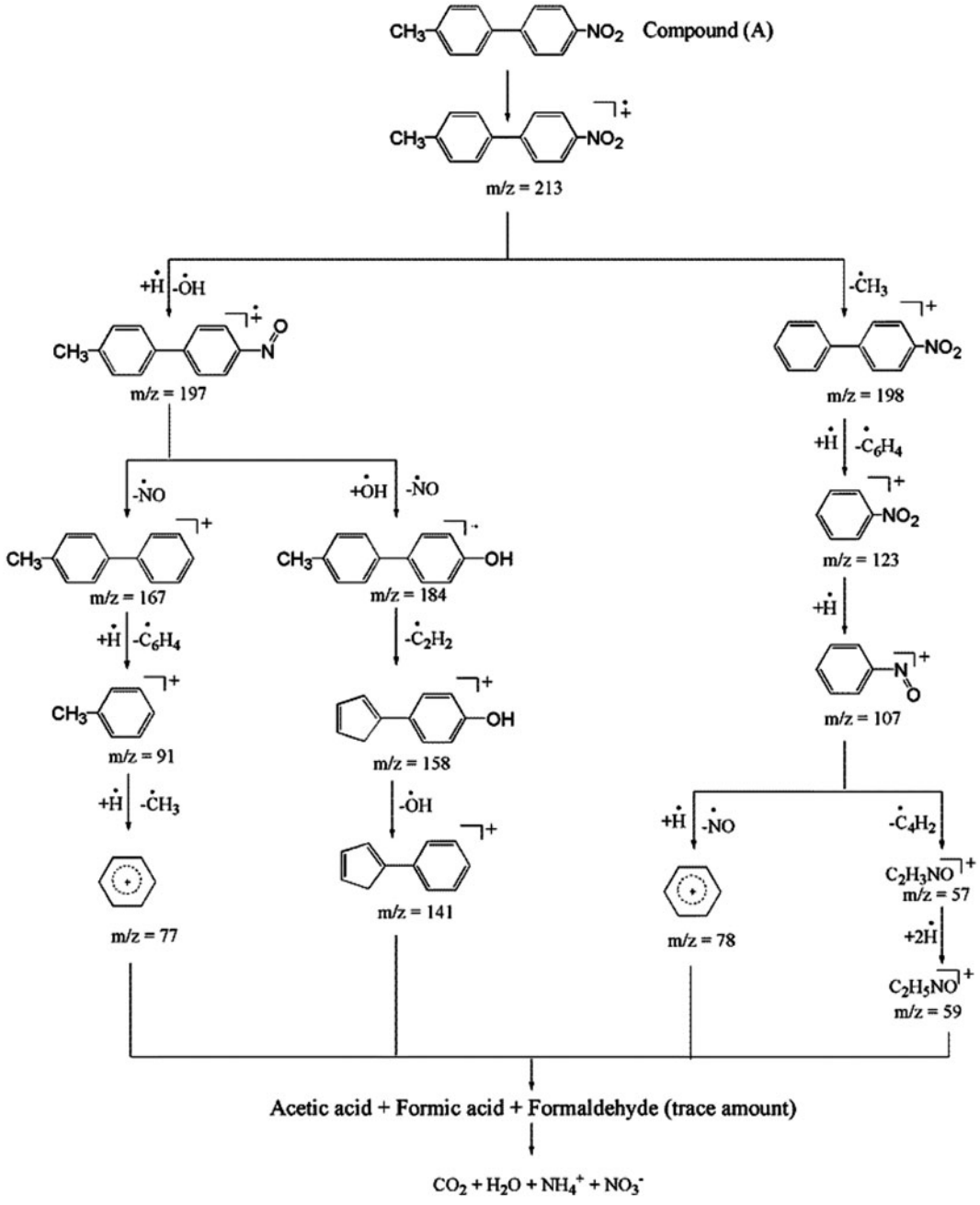

Fig. 6. Proposed fragmentation pattern of 4-methyl-4´´-nitrobiphenyl.

irradiation, some intermediates were present together with the unreacted substrate.

All the starting structures involved, and intermediates, detected by ESI-MS and HPLC are considered in Figs. 5 and 6 and demonstrate the plausible fragmentation path and intermediates. Although not quantified precisely, some of the proposed intermediates were clearly identified. Fig. 5 starts with the parental PNT molecule. The mineralization of this parental molecule can occur by both oxidation and reduction processes as these are possible in heterogeneous photocatalysis in aqueous media.

The oxidation process is supposed to occur at methyl group which result in the formation of the intermediates shown in path "a" by removal and addition of different radicals mainly hydrogen and

hydroxyl radicals which are very common in this aqueous photocatalytic system. Apart from the preliminary transformation of the substrate, mainly involving their functional group, the progressive attack of the aromatic ring can be indicated by the detection of several hydroxylic and quinonoid derivatives [7,91,92].

The selectivity of the HO· radical attack to the aromatic ring in o-, m- and p- position strongly depend on the kind of substituent present on the ring [50]. The oxidation of this parent compound can produce the 4-nitrobenzaldehyde and 4-nitrobenzoic acid of $m/z = 151$ and 167, respectively. Further oxidation and decarboxylation of this 4-nitrobenzoic acid can give 4-nitro phenol ($m/z = 139$), phenol ($m/z = 94$) and nitrobenzene ($m/z = 123$), respectively. These compounds are believed to mineralize in CO_2, H_2O and NO_3^- by oxidation and removal of various possible radicals respectively. The intermediates resultants of reduction process are shown in path "b." The first step is the reduction of nitro group into amino group giving the m/z value 107. The 4-aminotoluene further can convert to 4-hydroxytoluene and 4-aminophenol by replacing amino and methyl groups by abundant hydroxyl groups, respectively. These intermediates also approach to complete mineralization by subsequently addition and removal of hydrogen, hydroxyl, and amino radicals. The intermediates suggested in this process are 4-hydroxytoluene, toluene, 4-aminophenol, and aniline having m/z values 108, 94, 109, and 93, respectively.

However, the peak at $m/z = 213$ is observed in all mass spectra. This peak in mass spectra is proposed by the formation of 4-methyl-4´-nitrobiphenyl (compound (A), Fig. 5). The proposal for 4-methyl-4´-nitrobiphenyl formation is feasible in aqueous media because in photocatalytic degradation of PNT, formation of toluene, and nitrobenzene radicals and their combination is common. The protonation of this compound followed by removal of methyl and hydroxyl groups gives the m/z values 198 and 197, respectively (Fig. 6). The peak of $m/z = 197$ further by removal of NO· radical can give the m/z value 167 and by hydroxylation of this compound at 184. The proposed compound of peak at 198 further can give peaks at 123, 107, and 78 by removal of benzene and further radicals, respectively. The last step involve oxidative opening of the aromatic ring, leading to small organic ions and inorganic species. These intermediates further attain mineralization by elimination of hydrocarbons, nitroso, nitro, and hydroxyl groups. The overall mineralization process is a multi-step and multi-directional which involves various intermediates and radicals formed during the process.

4. Conclusions

The study on the photocatalytic activity of TiO_2-coated NaY zeolite with and without silver ion exchange towards degradation and mineralization of *p*-nitrotoluene shows that the optimum loading of TiO_2 is required for the higher activity and the presence of silver ion enhances the photocatalytic activity. The catalyst TiO_2/AgY2 with 2 w/w % loading of TiO_2 exhibited the highest photocatalytic activity for the degradation as well as the mineralization of *p*-nitrotoluene among the studied catalysts. The higher loading of TiO_2 can block the pores of zeolite material which results in decrease in adsorption capacity of *p*-nitrotoluene in the catalyst. This could make the decomposition less effective. The presence of the silver ion improves the charge separation and thus enhances the photocatalytic activity of TiO_2. The intermediates suggested were confirmed by the HPLC and decreasing COD values confirmed the mineralization occurring in the process. The kinetics of the photocatalytic oxidation of the *p*-nitrotoluene was successfully modeled by an approximation of the Langmuir–Hinshelwood (L–H) rate equation based on the hydroxyl radicals and direct hole attack. The reaction rate constants and adsorption constants were determined based on this L–H model.

Acknowledgement

This work was supported by Council of Scientific and Industrial Research, New Delhi, India under the Junior Research Fellowship Scheme (F.No. 10-2(5)/2005(i)-E.U.II).

References

[1] S. Ikeda, N. Sugiyama, B. Pal, G. Marcí, L. Palmisano, H. Noguchi, K. Uosaki, B. Ohtani, Photocatalytic activity of transition-metal-loaded titanium(IV) oxide powders suspended in aqueous solutions: Correlation with electron-hole recombination kinetics, Phys. Chem. Chem. Phys. 3 (2001) 267–273.
[2] A. Fuerte, M.D. Hernandez-Alonso, A.J. Maira, A. Martinez-Arias, M. Fernandez-Garcia, J.C. Conesa, J. Soria, Visible light-activated nanosized doped-TiO_2 photocatalysts, Chem. Commun. 24 (2001) 2718–2719.
[3] B.E. Haigler, J.C. Spain, Biotransformation of nitrobenzene by bacteria containing toluene degradative pathways, Appl. Environ. Microbiol. 57 (1991) 3156–3162.
[4] L.E. Hallas, M. Alexander, Microbial transformation of nitroaromatic compounds in sewage effluent, Appl. Environ. Microbiol. 45 (1983) 1234–1241.
[5] E.M. Davis, H.E. Murray, J.G. Liehr, E.L. Powers, Basic microbial degradation rates and chemical byproducts of selected organic compounds, Water Res. 15 (1981) 1125–1127.

[6] M. Rodriguez, V. Timokhin, F. Michl, S. Contreras, J. Gimenez, S. Esplugas, The influence of different irradiation sources on the treatment of nitrobenzene, Catal. Today 76 (2002) 291–300.
[7] P.K. Surolia, M.A. Lazar, R.J. Tayade, R.V. Jasra, Photocatalytic degradation of 3,3´-dimethylbiphenyl-4,4´-diamine (o-tolidine) over nanocrystalline TiO_2 synthesized by sol−gel, solution combustion, and hydrothermal methods, Ind. Eng. Chem. Res. 47 (2008) 5847–5855.
[8] D.F. Ollis, E. Pelizzetti, N. Serpone, Photocatalyzed destruction of water contaminants, J. Mol. Catal. A: Chem. 25 (1991) 1522–1529.
[9] M.R. Hoffmann, S.T. Martin, W.Y. Choi, D.W. Bahnemann, Environmental applications of semiconductor photocatalysis, Chem. Rev. 95 (1995) 69–96.
[10] J. Peral, X. Domènech, D.F. Ollis, Heterogeneous photocatalysis for purification, decontamination and deodorization of air, J. Porous Mater. 70 (1997) 117–140.
[11] M.A. Fox, K.E. Doan, M.T. Dulay, The effect of the "Inert" support on relative photocatalytic activity in the oxidative decomposition of alcohols on irradiated titanium dioxide composites, Res. Chem. Intermed. 20 (1994) 711–721.
[12] Y. Kim, M. Yoon, TiO_2/Y-zeolite encapsulating intramolecular charge transfer molecules: A new photocatalyst for photoreduction of methyl orange in aqueous medium, J. Mol. Catal. A: Chem. 168 (2001) 257–263.
[13] S.K. Lee, A. Mills, Detoxification of water by semiconductor photocatalysis, J. Ind. Eng. Chem. 10 (2004) 173–187.
[14] A. Mills, S.K. Lee, A web-based overview of semiconductor photochemistry-based current commercial applications, J. Photochem. Photobiol. A: Chem. 152 (2002) 233–247.
[15] D. Chakrabortty, S. Sen Gupta, Decolourisation of Metanil Yellow by visible-light photocatalysis with N-doped TiO_2 nanoparticles: Influence of system parameters and kinetic study, J. Phys. Chem. 52 (2013) 5528–5540.
[16] C.D. Wu, J.Y. Zhang, Y. Wu, G.Z. Wu, Degradation of phenol in water by the combination of sonolysis and photocatalysis, J. Phys. Chem. 52 (2014) 1911–1918.
[17] B. Sarwan, B. Pare, A.D. Acharya, S.B. Jonnalagadda, Mineralization and toxicity reduction of textile dye neutral red in aqueous phase using BiOCl photocatalysis, J. Phys. Chem. 116 (2012) 48–55.
[18] A. Pourtaheri, A. Nezamzadeh-Ejhieh, The role of the alkali metal co-cation in the ion exchange of Y zeolites IV. Cerium ion exchange equilibria, Microporous Mater. 137 (2015) 338–344.
[19] J. Augustynski, The role of the surface intermediates in the photoelectrochemical behaviour of anatase and rutile TiO_2, Electrochim. Acta 38 (1993) 43–46.
[20] H. Al-Ekabi, N. Serpone, Kinetics studies in heterogeneous photocatalysis. I. Photocatalytic degradation of chlorinated phenols in aerated aqueous solutions over titania supported on a glass matrix, J. Phys. Chem. 92 (1988) 5726–5731.
[21] M. Antonopoulou, D. Vlastos, I. Konstantinou, Photocatalytic degradation of pentachlorophenol by N–F–TiO_2: Identification of intermediates, mechanism involved, genotoxicity and ecotoxicity evaluation, J. Ind. Eng. Chem. 14 (2015) 520–527.
[22] U.G. Akpan, B.H. Hameed, Development and photocatalytic activities of TiO_2 doped with Ca–Ce–W in the degradation of acid red 1 under visible light irradiation, Catal. Today 52 (2013) 5639–5651.
[23] A. Nezamzadeh-Ejhieh, Z. Ghanbari-Mobarakeh, Heterogeneous photodegradation of 2,4-dichlorophenol using FeO doped onto nano-particles of zeolite P, J. Photochem. Photobiol. A: Chem. 21 (2015) 668–676.
[24] K.K. Akurati, S.S. Bhattacharya, M. Winterer, H. Hahn, Synthesis, characterization and sintering of nanocrystalline titania powders produced by chemical vapour synthesis, J. Phys. Chem. B 39 (2006) 2248–2254.
[25] A. Corma, H. Garcia, Zeolite-based photocatalysts, Chem. Commun. (2004) 1443–1459.
[26] Y. Kim, M. Yoon, TiO_2/Y-Zeolite encapsulating intramolecular charge transfer molecules: A new photocatalyst for photoreduction of methyl orange in aqueous medium, J. Mol. Cat. A: Chem. 168 (2001) 257–263.
[27] W. Wang, T. Yu, Y. Zeng, J. Chen, G. Yang, Y. Li, Enhanced photocatalytic hydrogen production from an MCM-41-immobilized photosensitizer-[Fe–Fe] hydrogenase mimic dyad, Photochem. Photobiol. Sci. 13 (2014) 1590–1597.
[28] K.W. Sing, Physisorption of nitrogen by porous materials, J. Porous Mater. 2 (1995) 5–8.
[29] A. Matsumoto, J.-X. Zhao, K. Tsutsumi, Adsorption behavior of hydrocarbons on slit-shaped micropores, Langmuir 13 (1997) 496–501.
[30] R.J. Tayade, R.G. Kulkarni, R.V. Jasra, Enhanced photocatalytic activity of TiO_2-coated NaY and HY zeolites for the degradation of methylene blue in water, Ind. Eng. Chem. Res. 46 (2006) 369–376.
[31] A. Nezamzadeh-Ejhieh, S. Khorsandi, Photocatalytic degradation of 4-nitrophenol with ZnO supported nano-clinoptilolite zeolite, J. Ind. Eng. Chem. 20 (2014) 937–946.
[32] A. Nezamzadeh-Ejhieh, M. Bahrami, Investigation of the photocatalytic activity of supported ZnO–TiO_2 on clinoptilolite nano-particles towards photodegradation of wastewater-contained phenol, Desalin. Water. Treat. 55 (2014) 1096–1104.
[33] K. Tsutsumi, H. Takahashi, Study of the nature of active sites on zeolites by the measurement of heat of immersion. I. Electrostatic field of calcium-substituted Y zeolite, J. Phys. Chem. 74 (1970) 2710–2713.
[34] K. Tsutsumi, H. Takahashi, Study of the nature of active sites on zeolites by the measurement of heat of immersion. II. Effects of silica/alumina ratio to electrostatic-field strength of calcium-exchanged zeolites, J. Phys. Chem. 76 (1972) 110–115.
[35] K.K. Iu, J.K. Thomas, Single-photon ionization of pyrene and anthracene giving trapped electrons in alkali-metal cation-exchanged zeolites X and Y: A direct time-resolved diffuse reflectance study, J. Phys. Chem. 95 (1991) 506–509.
[36] M.A. Keane, The role of the alkali metal co-cation in the ion exchange of Y zeolites IV. Cerium ion exchange equilibria, Microporous Mater. 7 (1996) 51–59.
[37] K.K. Iu, J.K. Thomas, Photophysical properties of pyrene in zeolites. 2. Effects of coadsorbed water, Langmuir 6 (1990) 471–478.

[38] A. Nezamzadeh-Ejhieh, Z. Banan, Photodegradation of dimethyldisulfide by heterogeneous catalysis using nano CdS and nano CdO embedded on the zeolite A synthesized from waste porcelain, Desalin. Water Treat. 52 (2013) 3328–3337.
[39] A. Nezamzadeh-Ejhieh, E. Shahriari, Photocatalytic decolorization of methyl green using Fe(II)-o-phenanthroline as supported onto zeolite Y, J. Ind. Eng. Chem. 20 (2014) 2719–2726.
[40] H.H. Patterson, R.S. Gomez, H. Lu, R.L. Yson, Nanoclusters of silver doped in zeolites as photocatalysts, Catal. Today 120 (2007) 168–173.
[41] M. Matsuoka, W.-S. Ju, H. Yamashita, M. Anpo, In situ characterization of the Ag^+ ion-exchanged zeolites and their photocatalytic activity for the decomposition of N_2O into N_2 and O_2 at 298 K, J. Photochem. Photobiol. A 160 (2003) 43–46.
[42] S.M. Kanan, M.C. Kanan, H.H. Patterson, Photophysical Properties of Ag(I)-exchanged Zeolite A and the photoassisted degradation of malathion, J. Phys. Chem. B 105 (2001) 7508–7516.
[43] E. Gachard, J. Belloni, M.A. Subramanian, Optical and EPR spectroscopic studies of silver clusters in Ag, Na–Y zeolite by [gamma]-irradiation, J. Mater. Chem. 6 (1996) 867–870.
[44] M. Anpo, M. Kondo, C. Louis, M. Che, S. Coluccia, Application of dynamic photoluminescence spectroscopy to the study of the active surface sites on supported molybdenum/silica catalysts: Features of anchored and impregnated catalysts, J. Am. Chem. Soc. 111 (1989) 8791–8799.
[45] T. Sun, K. Seff, Silver clusters and chemistry in zeolites, Chem. Rev. 94 (1994) 857–870.
[46] M. Anpo, S.G. Zhang, H. Mishima, M. Matsuoka, H. Yamashita, Design of photocatalysts encapsulated within the zeolite framework and cavities for the decomposition of NO into N_2 and O_2 at normal temperature, Catal. Today 39 (1997) 159–168.
[47] R.J. Tayade, P.K. Surolia, M.A. Lazar, R.V. Jasra, Enhanced photocatalytic activity by silver metal ion exchanged NaY zeolite photocatalysts for the degradation of organic contaminants and dyes in aqueous medium, Ind. Eng. Chem. Res. 47 (2008) 7545–7551.
[48] M. Shariq Vohra, K. Tanaka, Photocatalytic degradation of nitrotoluene in aqueous TiO_2 suspension, Water Res. 36 (2002) 59–64.
[49] P. Piccinini, C. Minero, M. Vincenti, E. Pelizzetti, Photocatalytic interconversion of nitrogen-containing benzene derivatives, J. Chem. Soc., Faraday Trans. 93 (1997) 1993–2000.
[50] G. Palmisano, V. Loddo, V. Augugliaro, L. Palmisano, S. Yurdakal, Photocatalytic oxidation of nitrobenzene and phenylamine: Pathways and kinetics, AIChE J. 53 (2007) 961–968.
[51] S.P. Kamble, S.B. Sawant, J.C. Schouten, V.G. Pangarkar, Photocatalytic and photochemical degradation of aniline using concentrated solar radiation, J. Chem. Technol. Biotechnol. 78 (2003) 865–872.
[52] C. Karunakaran, S. Senthilvelan, Solar photocatalysis: Oxidation of aniline on CdS, Sol. Energy 79 (2005) 505–512.
[53] A.N. Ejhieh, M. Khorsandi, Photodecolorization of Eriochrome Black T using NiS–P zeolite as a heterogeneous catalyst, J. Hazard. Mater. 176 (2010) 629–637.
[54] A. Nezamzadeh-Ejhieh, S. Hushmandrad, Solar photodecolorization of methylene blue by CuO/X zeolite as a heterogeneous catalyst, Appl. Catal. A: Gen. 388 (2010) 149–159.
[55] A. Nezamzadeh-Ejhieh, Z. Banan, Sunlight assisted photodecolorization of crystal violet catalyzed by CdS nanoparticles embedded on zeolite A, Desalination 284 (2012) 157–166.
[56] A. Nezamzadeh-Ejhieh, M. Amiri, CuO supported clinoptilolite towards solar photocatalytic degradation of p-aminophenol, Powder Technol. 235 (2013) 279–288.
[57] H. Tran, K. Chiang, J. Scott, R. Amal, Understanding selective enhancement by silver during photocatalytic oxidation, Photochem. Photobiol. Sci. 4 (2005) 565–567.
[58] H. Yang, F. Chen, Y. Jiao, J. Zhang, The role of interfacial lattice Ag^+ on titania based photocatalysis, Appl. Catal. B: Environ. 130–131 (2013) 218–223.
[59] P. Madeira, M.R. Nunes, C. Borges, F.M.A. Costa, M.H. Florêncio, Benzidine photodegradation: A mass spectrometry and UV spectroscopy combined study, Rapid Commun. Mass Spectrom. 19 (2005) 2015–2020.
[60] M.H. Florêncio, E. Pires, A.L. Castro, M.R. Nunes, C. Borges, F.M. Costa, Photodegradation of Diquat and Paraquat in aqueous solutions by titanium dioxide: Evolution of degradation reactions and characterisation of intermediates, Chemosphere 55 (2004) 345–355.
[61] Y. Cao, L. Yi, L. Huang, Y. Hou, Y. Lu, Mechanism and pathways of chlorfenapyr photocatalytic degradation in aqueous suspension of TiO_2, Environ. Sci. Technol. 40 (2006) 3373–3377.
[62] S. Malato, J. Cáceres, A.R. Fernández-Alba, L. Piedra, M.D. Hernando, A. Agüera, J. Vial, Photocatalytic treatment of diuron by solar photocatalysis: Evaluation of main intermediates and toxicity, Environ. Sci. Technol. 37 (2003) 2516–2524.
[63] S. Song, M. Xia, Z. He, H. Ying, B. Lü, J. Chen, Degradation of p-nitrotoluene in aqueous solution by ozonation combined with sonolysis, J. Hazard. Mater. 144 (2007) 532–537.
[64] F.J. Beltrán, J.M. Encinar, M.A. Alonso, Nitroaromatic hydrocarbon ozonation in water. 1. Single ozonation, Ind. Eng. Chem. Res. 37 (1998) 25–31.
[65] J. Sarasa, M.P. Roche, M.P. Ormad, E. Gimeno, A. Puig, J.L. Ovelleiro, Treatment of a wastewater resulting from dyes manufacturing with ozone and chemical coagulation, Water Res. 32 (1998) 2721–2727.
[66] O.A. Sadik, D.M. Witt, Peer reviewed: Monitoring endocrine-disrupting chemicals, Environ. Sci. Technol. 33 (1999) 368A–374A.
[67] P.K. Surolia, R.J. Tayade, R.V. Jasra, TiO_2-coated cenospheres as catalysts for photocatalytic degradation of methylene blue, p-nitroaniline, n-decane, and n-tridecane under solar irradiation, Ind. Eng. Chem. Res. 49 (2010) 8908–8919.
[68] H. Chen, A. Matsumoto, N. Nishimiya, K. Tsutsumi, Preparation and characterization of TiO_2 incorporated Y-zeolite, Colloids Surf., A 157 (1999) 295–305.
[69] G.J. Ray, A.G. Nerheim, J.A. Donohue, Characterization of defects in dealuminated faujasite, Zeolites 8 (1988) 458–463.
[70] S. van Donk, A.H. Janssen, J.H. Bitter, K.P. de Jong, Generation, characterization, and impact of mesopores in zeolite catalysts, Catal. Rev. 45 (2003) 297–319.

[71] G. Cosa, M.S. Galletero, L. Fernandez, F. Marquez, H. Garcia, J.C. Scaiano, Tuning the photocatalytic activity of titanium dioxide by encapsulation inside zeolites exemplified by the cases of thianthrene photooxygenation and horseradish peroxidase photodeactivation, New J. Chem. 26 (2002) 1448–1455.
[72] G.A. Ozin, H. Huber, Cryophotoclustering techniques for synthesizing very small, naked silver clusters Agn of known size (where $n = 2–5$). The molecular metal cluster-bulk metal particle interface, Inorg. Chem. 17 (1978) 155–163.
[73] G.A. Ozin, F. Hugues, S.M. Mattar, D.F. McIntosh, Low nuclearity silver clusters in faujasite-type zeolites: Optical spectroscopy, photochemistry and relationship to the photodimerization of alkanes, J. Phys. Chem. 87 (1983) 3445–3450.
[74] Y. Kim, K. Seff, Structure of a very small piece of silver metal. The octahedral silver (Ag6) molecule. Two crystal structures of partially decomposed vacuum-dehydrated fully silver(1+) ion-exchanged zeolite A, J. Am. Chem. Soc. 99 (1977) 7055–7057.
[75] C. Shi, M. Cheng, Z. Qu, X. Bao, Investigation on the catalytic roles of silver species in the selective catalytic reduction of NO_x with methane, Appl. Catal. B: Environ. 51 (2004) 171–181.
[76] K.-I. Shimizu, J. Shibata, H. Yoshida, A. Satsuma, T. Hattori, Silver-alumina catalysts for selective reduction of NO by higher hydrocarbons: Structure of active sites and reaction mechanism, Appl. Catal. B: Environ. 30 (2001) 151–162.
[77] K.-I. Shimizu, A. Satsuma, Selective catalytic reduction of NO over supported silver catalysts-practical and mechanistic aspects, Phys. Chem. Chem. Phys. 8 (2006) 2677–2695.
[78] S. Naskar, S. Arumugom Pillay, M. Chanda, Photocatalytic degradation of organic dyes in aqueous solution with TiO_2 nanoparticles immobilized on foamed polyethylene sheet, J. Photochem. Photobiol., A 113 (1998) 257–264.
[79] H.M. Sung-Suh, J.R. Choi, H.J. Hah, S.M. Koo, Y.C. Bae, Comparison of Ag deposition effects on the photocatalytic activity of nanoparticulate TiO_2 under visible and UV light irradiation, J. Photochem. Photobiol., A 163 (2004) 37–44.
[80] M. Andersson, H. Birkedal, N.R. Franklin, T. Ostomel, S. Boettcher, A.E.C. Palmqvist, G.D. Stucky, Ag/AgCl-loaded ordered mesoporous anatase for photocatalysis, Chem. Mater. 17 (2005) 1409–1415.
[81] P.K. Surolia, R.V. Jasra, Degradation and mineralization of aqueous nitrobenzene using ETS-4 photocatalysis, Desalin. Water Treat. (2015), 1–10, doi: 10.1080/19443994.2015.1079801.
[82] G. Mills, M.R. Hoffmann, Photocatalytic degradation of pentachlorophenol on titanium dioxide particles: Identification of intermediates and mechanism of reaction, Environ. Sci. Technol. 27 (1993) 1681–1689.
[83] Y. Mao, C. Schoeneich, K.D. Asmus, Identification of organic acids and other intermediates in oxidative degradation of chlorinated ethanes on titania surfaces en route to mineralization: A combined photocatalytic and radiation chemical study, J. Phys. Chem. 95 (1991) 10080–10089.
[84] P.K. Surolia, R.J. Tayade, R.V. Jasra, Effect of anions on the photocatalytic activity of Fe(III) salts impregnated TiO_2, Ind. Eng. Chem. Res. 46 (2007) 6196–6203.
[85] A. Sclafani, J.-M. Herrmann, Influence of metallic silver and of platinum-silver bimetallic deposits on the photocatalytic activity of titania (anatase and rutile) in organic and aqueous media, J. Photochem. Photobiol., A 113 (1998) 181–188.
[86] A. Sclafani, M.-N. Mozzanega, J.-M. Herrmann, Influence of silver deposits on the photocatalytic activity of titania, J. Catal. 168 (1997) 117–120.
[87] A. Dobosz, A. Sobczyński, The influence of silver additives on titania photoactivity in the photooxidation of phenol, Water Res. 37 (2003) 1489–1496.
[88] V. Vamathevan, R. Amal, D. Beydoun, G. Low, S. McEvoy, Silver metallisation of titania particles: Effects on photoactivity for the oxidation of organics, Chem. Eng. J. 98 (2004) 127–139.
[89] A. Bansal, S. Madhavi, T.T.Y. Tan, T.M. Lim, Effect of silver on the photocatalytic degradation of humic acid, Catal. Today 131 (2008) 250–254.
[90] B. Xin, L. Jing, Z. Ren, B. Wang, H. Fu, Effects of simultaneously doped and deposited Ag on the photocatalytic activity and surface states of TiO_2, J. Phys. Chem. B 109 (2005) 2805–2809.
[91] C. Minero, E. Pelizzetti, P. Piccinini, M. Vincenti, Photocatalyzed transformation of nitrobenzene on TiO_2 and ZnO, Chemosphere 28 (1994) 1229–1244.
[92] V. Augugliaro, L. Palmisano, A. Sclafani, C. Minero, E. Pelizzetti, Photocatalytic degradation of phenol in aqueous titanium dioxide dispersions, Toxicol. Environ. Chem. 16 (1988) 89–109.

Appendix A

In the mechanism presented in Section 3.2, there are four possibilities of the mineralization shown from Eqs. (9)–(12). Out of these four possibilities, we can select Eq. (11) for kinetic study. There are two reasons behind it:

(1) The intermediates are in very less concentration as compared to initial compound PNT, showing the less possibility of reaction (10) and (12).
(2) By the reaction–diffusion model, the average rate of reaction between photogenerated ·OH and semiconductor surface is far less than the diffusion rate. Thus, it is plausible for the radical to diffuse away from the surface and to react subsequently in solution with less possibility of Eq. (9).

So the case of Eq. (11) is a typical mechanism since the surface ·OH group must diffuse into solution and the organic reactant PNT must adsorb on catalytic surface after generation in bulk phase. Thus, the rate disappearance of reactant PNT may be represented as:

$$r_{PNT} = k_{11}[^{\cdot}OH][> TiO_2\text{–}PNT] \tag{A1}$$

The surface concentration of PNT, intermediates, and radical can be obtained by the adsorption equilibrium so from Eqs. (4)–(6):

$$ > TiO_2\text{–}PNT = K_P[> TiO_2][PNT] \tag{A4}$$

$$ > TiO_2\text{–}I = K_I[> TiO_2][I] \tag{A5}$$

$$ > TiO_2\text{–}^{\cdot}OH = K_{OH}[> TiO_2][^{\cdot}OH] \tag{A6}$$

where $K_P = k_4/k_{-4}$, $K_I = k_5/k_{-5}$ and $K_{OH} = k_6/k_{-6}$.

Using the values of (A4)–(A6), Eq. (A3) can be written as:

$$\begin{aligned}\frac{d[^{\cdot}OH]}{dt} = {} & k_3'\left[h_{VB}^+\right] - k_{-3}K_{OH}[TiO_2][^{\cdot}OH] \\ & - k_{11}K_P[TiO_2][PNT][^{\cdot}OH] \\ & - \sum_{i=1}^{n} k_i K_{OH}[\,TiO_2][I][^{\cdot}OH]\end{aligned} \tag{A7}$$

Thus, the bulk ·OH radical can be obtained by applying quasi-steady state approximation on Eq. (A7):

$$[^{\cdot}OH] = \frac{k_3'\left[h_{VB}^+\right]}{k_{-3}K_{OH}[> TiO_2] + k_{11}K_P[> TiO_2][PNT] + \sum_{i=1}^{n} k_i K_I[> TiO_2][I]} \tag{A8}$$

The balance for the total ·OH radical concentration from above discussion can be written as:

$$\begin{aligned}\frac{d[^{\cdot}OH]}{dt} = {} & k_3[> TiO_2\text{–}OH^-]\left[h_{VB}^+\right] \\ & - k_{-3}[> TiO_2\text{–}^{\cdot}OH]k_{11}[> TiO_2\text{–}PNT][^{\cdot}OH] \\ & - \sum_{i=1}^{n} k_i[> TiO_2\text{–}I][^{\cdot}OH]\end{aligned} \tag{A2}$$

However, the concentration of [>TiO_2–OH^-] should be relatively constant in aqueous media as in Eq. (3), equilibrium lies far to right. So taking this:

$$\begin{aligned}\frac{d[^{\cdot}OH]}{dt} = {} & k_3'\left[h_{VB}^+\right] - k_{-3}[> TiO_2\text{–}^{\cdot}OH] \\ & - k_{11}[> TiO_2\text{–}PNT][^{\cdot}OH] \\ & - \sum_{i=1}^{n} k_i[> TiO_2\text{–}I][^{\cdot}OH]\end{aligned} \tag{A3}$$

Here "*n*" represents the number of different organic intermediate species present. Similarly, the h^+ concentration balance by quasi steady state approximation can be written as:

$$\begin{aligned}\frac{d[H^+]}{dt} = {} & k_1[> TiO_2] - k_2\left[h_{VB}^+\right]\left[e_{CB}^-\right] \\ & - k_3[> TiO_2\text{–}OH^-]\left[h_{VB}^+\right] + k_{-3}[> TiO_2\text{–}^{\cdot}OH]k_7 \\ & - [> TiO_2\text{–}PNT]\left[h_{VB}^+\right] - k_8[> TiO_2\text{–}I]\left[h_{VB}^+\right]\end{aligned} \tag{A9}$$

However, the photogenerated holes are removed by recombination faster than any other trapping process [42,47], so considering this Eq. (A9) can be written as:

$$\frac{d[H^+]}{dt} = k_1[> TiO_2] - k_2\left[h_{VB}^+\right]\left[e_{CB}^-\right] \tag{A10}$$

As the photogeneration rate of h^+ and e^- are equal, then we can assume that $[h^+] = [e^-]$, using this and by applying quasi-steady state approximation, the hole concentration from Eq. (A10):

$$[h^+_{VB}] = [k_1/k_2]^{1/2}[> TiO_2]^{1/2} \quad (A11)$$

Putting this value in Eq. (A8):

$$[^{\cdot}OH] = \frac{k'_3\left[\frac{k_1}{k_2}\right]^{1/2}[> TiO_2]^{1/2}}{k_{-3}K_{OH}[> TiO_2] + k_{11}K_P[> TiO_2][PNT] + \sum_{i=1}^{n} k_iK_I[> TiO_2][I]} \quad (A12)$$

Using the Eq. (A12) in Eq. (A1), the rate of PNT degradation:

$$r_{PNT} = \frac{k_{11}K_P[> TiO_2][PNT] \cdot k'_3\left[\frac{k_1}{k_2}\right]^{1/2}[> TiO_2]^{1/2}}{k_{-3}K_{OH}[> TiO_2] + k_{11}K_P[> TiO_2][PNT] + \sum_{i=1}^{n} k_iK_I[> TiO_2][I]} \quad (A13)$$

$$r_{PNT} = \frac{kK[PNT]}{1 + K[PNT] + \sum_{i=1}^{n} K_i[I]} \quad (A14)$$

where $k = k'_3[k_1/k_2]^{1/2}$, $K = \frac{k_{11}K_P}{k_{-3}K_{OH}}$, $K_i = \frac{k_iK_I}{k_{-3}K_{OH}}$.

k is the reaction kinetic constant (mol L^{-1} min^{-1}) and K (L mol^{-1}) is the adsorption constant of reactant PNT. K_i (L mol^{-1}) is the adsorption constant of intermediate products adsorbed on catalyst surface. Since the adsorption constant and concentration on intermediates are difficult to measure, two distinct approximations can be made [76,77].

Approximation (1): The concentration of intermediates adsorbed on the catalyst surface can be neglected as compared to primary substrate PNT, and then Eq. (A14) can be simplified as:

$$r_{PNT} = \frac{kK[PNT]}{1 + K[PNT]} \quad (A15)$$

This is assumed to be valid for very low degree of conversion.

Approximation (2): The photocatalytic degradation process is a stepwise process where adsorption constant of intermediates and main substrate (PNT) are the same $K_{i=1} = K_{i=2} = \text{———} = K_{i=n} = K$, thus Eq. (A14) becomes:

$$r_{PNT} = \frac{kK[PNT]}{1 + K[PNT]_0} \quad (A16)$$

where $[PNT]_0$ represent the initial concentration of reactant PNT.

Since in initial condition $[PNT] = [PNT]_0$, then using Eq. (A15):

$$\frac{1}{r_{PNT}} = \frac{1}{k} + \frac{1}{kK} \cdot \frac{1}{[PNT]_0} \quad (A17)$$

From the plot of $1/r_{PNT}$ vs. $1/[PNT]_0$, we can get the values of k and K. All the parameters were determined using the initial rates and initial concentration data where the effect of the intermediates can be conveniently neglected (Approximation 2). The intercept determines the reaction kinetic constant "k" that varies with the rate of degradation and the value of adsorption constant "K" can be obtained by the slope of the curve.